Structure and Properties Development in Poly(phenylene sulfide) Fibers. II. Effect of One-Zone Draw Annealing

Prabhakar Gulgunje, Gajanan Bhat, Joseph Spruiell

Department of Materials Science and Engineering, The University of Tennessee, Knoxville 37996

Received 31 October 2010; accepted 27 July 2011
DOI 10.1002/app.35377
Published online 18 January 2012 in Wiley Online Library (wileyonlinelibrary.com).

ABSTRACT: In this article, we discuss the role of one-zone drawing followed by annealing in enhancing the structure and properties of fibers manufactured from Fortron® linear poly(phenylene sulfide) resins. The interaction effects of the polymer molecular weight (MW), melt-spinning process parameters, and draw-annealing process conditions were also elucidated. Several tools used to probe the investigation were tensile testing, differential scanning calorimetry, polarized light optical microscopy, wide-angle X-ray scattering, and small-angle X-ray scattering. This study showed that the optimum drawing temperature was around 95°C. A considerable improvement in the fiber tensile properties was observed upon drawing and annealing under optimum processing conditions. Fibers with tenacities close to 5 g/den were obtained. The development of the tensile properties was statistically correlated with the morphological changes in the fibers. The routes to achieving fibers with optimum tensile properties were shown to be different for resins with different MWs.
© 2012 Wiley Periodicals, Inc. J Appl Polym Sci 125: 1890–1900, 2012

Key words: fibers; structure-property relations; high performance polymers; extrusion; WAXS

INTRODUCTION

Several researchers have investigated the crystallization kinetics of poly(phenylene sulfide) (PPS),[1] the interest of which mainly stems from high consumption of PPS in the manufacture of injection-molded components. However, very few investigators have reported the structure–property development in PPS melt-spun and drawn fibers.

Song et al.[2] studied the melt spinning of Ryton® PPS with an Instron capillary rheometer and performed drawing over a hot plate. Using industrially produced multifilament PPS as-spun yarns, Carr and Ward[3] reported the optimum drawing temperature (DT) to be close to the glass-transition temperature of the polymer. Drawing below 80°C resulted in voids, and the yarn stuck to the draw rolls when it was drawn above 100°C. After a single-stage drawing process, the birefringence (Δn) of PPS reached 0.208 and was close to 0.27 after annealing. They reported that the initial modulus of PPS fibers drawn at 80°C was equal to 8 GPa and the failure stress was equal to 740 MPa, which was lower than that of poly(ethylene terephthalate).[4] Because the level of orientation achieved in the yarns was close to the intrinsic birefringence (Δ^o), equal to 0.31, they deduced, on the basis of the shrinkage force measurement and bond polarizabilities of PPS, that the entanglement density was higher in case of PPS than in poly(ethylene terephthalate).

The drawing of melt-spun fibers produced from Fortron® PPS resins was reported by Krins et al.[5] Using steam-assisted multizone drawing and annealing, they reported a fiber tenacity close to 60 cN/tex (6 g/den), an elongation at break around 18%, and a Young's modulus around 400–450 cN/tex at 0.5–2% extension. Bratukhin et al.[6] reported that drawing in pressurized steam resulted in the best physicochemical properties in polypropylene fibers. The high coefficient of heat transfer, the absence of an oxidizing agent, and the plasticizing effect produced by water in the vapor form were reported to lead to better properties in the fibers.

In a study of Ryton® PPS fibers, Murthy et al.[7] found that with an increase in the annealing temperature (AT) from 100 to 285°C, the lamellar spacing determined by small-angle X-ray scattering (SAXS) and the crystal size based on the (110) and (200) planes determined by wide-angle X-ray scattering (WAXS) increased.

Suzuki et al.[8] employed the zone-drawing and zone-annealing technique to improve the mechanical properties of PPS fibers. The optimum drawing and annealing conditions were observed at temperatures of 90 and 220°C, respectively. Annealing was carried out under tension at 138 MPa. The tensile strength and modulus of the fibers were reported to be around 0.7 and 8 GPa, respectively. They reported an increase in the crystalline orientation factor (f_c) to 0.982 after zone drawing and a further small increase to 0.986 after zone annealing.

Correspondence to: G. Bhat (gbhat@utk.edu).

© 2012 Wiley Periodicals, Inc.

With these limited studies on fibers, this research was conducted to elucidate the relationship between the polymer molecular weight (MW) and the fiber spinning and postprocessing conditions on the morphological development, which determine the tensile properties of draw-annealed fibers. In this study, we focused on the role of one-zone draw annealing (DA) and the interaction effects of material and processing variables upon the structure–property development in the fibers.

EXPERIMENTAL

The details of the materials and experimental methods used to manufacture as-spun fibers were reported in our earlier publication.[9] The methods relevant to this investigation and not discussed in the prior publication are discussed herein.

One-zone drawing and annealing

The draw unit supplied by SAHM winders, Eschwege, Germany, shown in Figure 1, was used for the purposes of drawing the as-spun yarns. Throughout these experiments, the draw ratio employed was the maximum achievable for each of the yarns to yield satisfactory drawing without yarn breakage. The total draw ratio was employed between the first and second draw rolls. The temperatures of the draw rolls were varied in the range 85–120°C in steps of 5°C. Annealing was carried out with a 4 in. long heater, which was placed between the second and third draw-roll pairs, as shown in Figure 1. The temperature of the annealing heater was maintained such that the temperature of the air very close to the inside surface was around 150°C. The draw-annealed yarns were wound on the package with a winder.

Fiber characterization

The details of characterization of the fiber properties, such as the denier, tensile strength, breaking elongation, tensile modulus, overall molecular orientation, and degree of crystallinity as determined by differential scanning calorimetry (DSC), were discussed in detail in our earlier publication.[9]

Morphological evaluations

Crystallinity

WAXS pinhole patterns of the draw-annealed fiber samples that were obtained as discussed in our earlier publication[9] were converted into 2θ versus intensity data with Polar software (Precision Works NY, Inc., East Setauket, NY). Because the calculation of the crystallinity index by this technique requires the knowledge of the contribution due to the amorphous fraction, an amorphous film was made from

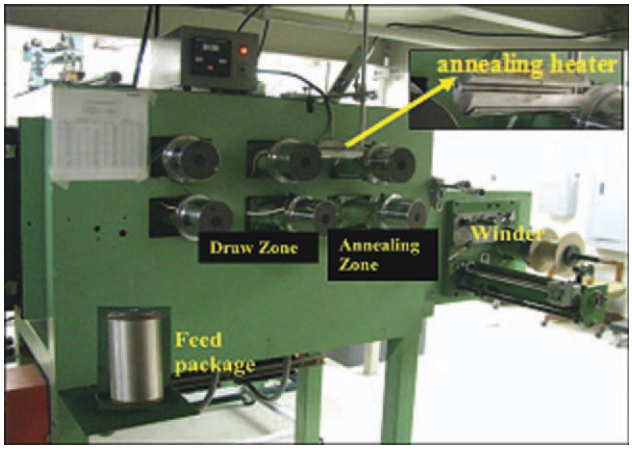

Figure 1 Picture of the zone draw-annealing unit. [Color figure can be viewed in the online issue, which is available at wileyonlinelibrary.com.]

polymer 3P by hot pressing at 325°C and then by cooling rapidly using an ice-water bath. The film thus made possessed very little crystallinity when analyzed by DSC. Its pinhole pattern, obtained with WAXS, showed an essentially amorphous nature [Fig. 2(a)]. From the 2θ versus intensity data from the Polar software supplied by precision works, Inc., East Setauket, NY, with the software Peakfit 4.0 (Systat Software, Inc., San Jose, CA), the multiple peaks in the diffraction patterns were deconvoluted into peaks at various 2θ values. The peak-fitted plot of the amorphous film is shown in Figure 2(b). Using Rietveld modeling, Morton et al.[10] reported multiple (3–4) peaks corresponding to amorphous fractions in PPS. Similar treatment seemed to fit well in these experiments for the amorphous film, and hence, three broad peaks were assigned to contributions due to the amorphous fraction, and the small narrow peak at 2θ equal to 18.7° was assigned a contribution due to the crystalline fraction. Figure 3 shows the nature of the diffractogram corresponding to the completely amorphous fraction after the combination of multiple peaks associated with it. For the purpose of clarity, the amorphous background is separated in the figure from the original curve. The crystallinity index (X) thus obtained with Eq. (1) was fairly close to that determined by DSC. In the analysis of the crystallinity index of PPS draw-annealed fibers, similar treatment was given to assign the amorphous fraction contributions, and then, the remaining portion of the diffractogram was considered to be the contribution due to the crystalline fraction:

$$X = \frac{I_c}{I_c + I_a} \times 100 \quad (1)$$

where I_c is the sum of diffraction intensities due to the crystalline fraction and I_a is the sum of diffraction intensities due to the amorphous fraction. It is

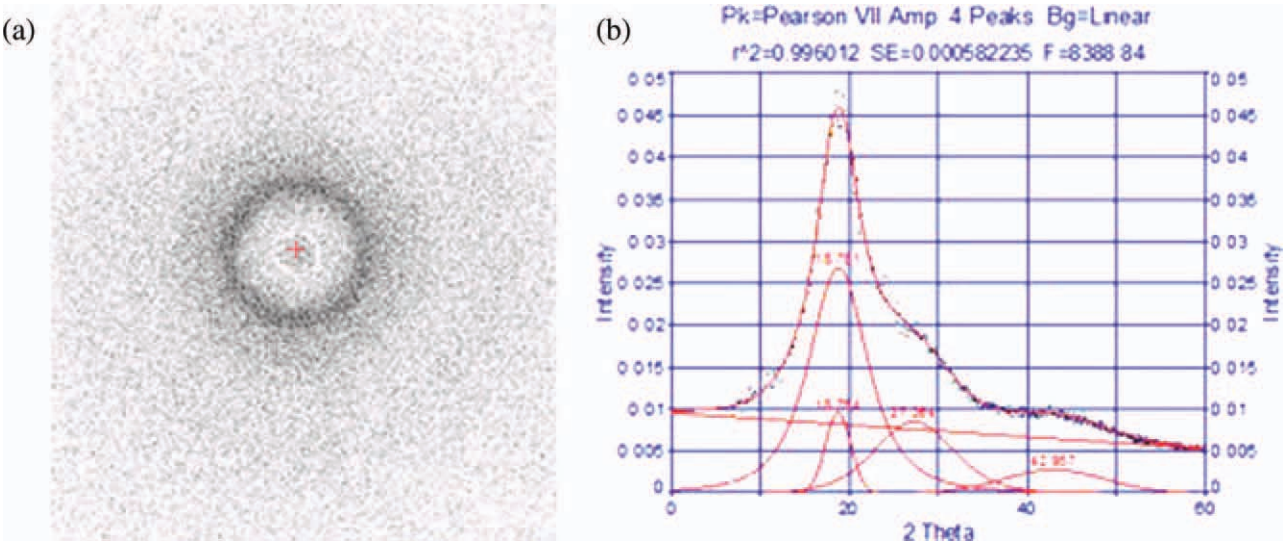

Figure 2 Amorphous film: (a) WAXS pinhole pattern and (b) peak-fitted curve. [Color figure can be viewed in the online issue, which is available at wileyonlinelibrary.com.]

to be noted that the crystallinities determined by DSC and WAXS were used as relative values to explain the effect of the processing parameters and cannot be considered as absolute numbers.

Molecular orientation

Overall orientation. The overall orientation was determined by birefringence (Δn) with a polarized optical microscope (Prior Scientific Inc., Rockland, MA) equipped with compensator. The details of Δn measurement were reported in our earlier publication.[9]

Crystalline orientation. Tabor et al.[11] reported that the crystal structure of PPS is orthorhombic. Therefore, a minimum of two planes are required to calculate $\langle \cos^2 \phi_{hkl} \rangle$, where ϕ_{hkl} is the angle between normal to plane (hkl) & fiber axis.[12] The pinhole patterns obtained with WAXS, as discussed previously, were evaluated for azimuthal intensities corresponding to $2\theta = 18.8$ and 20.4°; these values represent the crystal planes (110) and (200), respectively. From the azimuthal intensity distribution of plane (*hkl*) perpendicular to the crystallographic axis, the $\langle \cos^2 \phi_{hkl} \rangle$ value for each of the above planes was calculated with Eq. (2).[13] The overlapping crystal planes (200) and (111) at $2\theta = 20.4$ and 20.6°, respectively, were deconvoluted into two peaks with the Peakfit 4.0 software to determine the intensities corresponding to each of these reflections. Equation (3) was derived to calculate $\cos^2 \phi_{c,z}$, where $\phi_{c,z}$ is the angle between the polymer chain axis & the fiber axis, along the fiber axis based on the (110) and (200) planes:

$$\langle \cos^2 \phi_{hkl} \rangle = \frac{\int_0^{\pi/2} I_{hkl}(\phi) \cos^2 \phi \sin \phi d\phi}{\int_0^{\pi/2} I_{hkl}(\phi) \sin \phi d\phi} \quad (2)$$

where I_{hkl} is the intensity of plane *hkl*.

$$\cos^2 \phi_{c,z} = 1 - \left(0.5813X \cos^2 \phi_{200,z} + 1.4187X \cos^2 \phi_{110,z}\right) \quad (3)$$

The values of $\cos^2 \phi_{c,z}$ calculated from Eq. (3) were used in Eq. (4)[14] to calculate Herman's orientation factor for the crystalline regions.

$$f_c = \frac{3\cos^2 \phi_c - 1}{2} \quad (4)$$

where ϕ_c is the angle between the crystallographic axis (polymer chain axis) and the fiber axis.

Amorphous orientation. From f_c and Δn obtained for each of the fibers as discussed previously, the amorphous orientation factor (f_{am}) was calculated using Eq. (5):[15,16]

$$\Delta n = X f_c \Delta_c^o + (1 - X) f_{am} \Delta_{am}^o + \Delta n_{\text{form}} \quad (5)$$

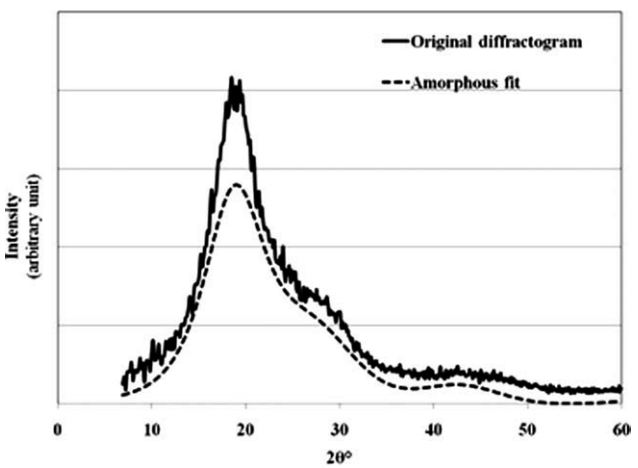

Figure 3 Amorphous peak fit in the amorphous PPS film.

where f is the orientation factor, the subscripts c and am stand for the crystalline and amorphous regions, respectively, Δ^o is the intrinsic birefringence of PPS of corresponding forms, and Δn_{form} is the form birefringence, which is usually considered negligible.

For PPS, a Δ^o equal to 0.27 was reported by Maemura et al.,[17] whereas, Carr and Ward[18] reported it to be 0.333. The level of Δn measured in the PPS fibers in this research was up to 0.31, and hence, Δ^o reported by Carr and Ward[18] was considered herein. Using eqs. (6),[17] (7),[19] and (8),[19] we calculated Δ_c^o and Δ_{am}^o to be around 0.3463 and 0.3197, respectively:

$$\Delta^o = \frac{\Delta_c^o + \Delta_{am}^o}{2} \tag{6}$$

$$\Delta_c^o = k\rho_c \tag{7}$$

$$\Delta_{am}^o = k\rho_{am} \tag{8}$$

where k is a constant. A density of 100% crystalline PPS (ρ_c) equal to 1.43 g/cm^3 and a density of 100% amorphous PPS (ρ_{am}) equal to 1.32 g/cm^3, respectively, as reported by Tabor et al.,[11] was considered.

Crystal size. From the WAXS pattern, the mean crystallite size was determined with the Scherrer[20,21] equation, as given by Eq. (9):

$$L_{hkl} = \frac{K\lambda}{\beta_0 \cos\theta} \tag{9}$$

where L_{hkl} is the mean dimension of the crystallite perpendicular to the plane (hkl), β_0 is the full width at half-maximum (also abbreviated as FWHM) of the (hkl) reflection (rad), K is a constant and is considered to be 0.9, and θ is one-half the diffraction angle corresponding to plane (hkl). The crystal size thus obtained on the basis of reflections from planes (110) and (200) was termed as the crystal width.

A correction due to instrumental broadening (b) was applied to the measured fwhm (B) corresponding to plane (hkl) to determine β_0. Equation (10) was used to apply the correction:[22]

$$\beta_0^2 = B^2 - b^2 \tag{10}$$

To obtain fwhm (B) of the two strong reflections from planes (110) and (200), the WAXS pinhole patterns were evaluated with the Polar software for X-axis scans with the Y coordinate at the center and with a line width of 15 pixels, where the pixel size was 0.05 mm. While peak fitting the intensity versus 2θ profiles in Peakfit 4.0 software, for peaks at 2θ equal to 18.8 and 20.4°, the contribution due to amorphous scattering in the profiles was peak-fitted. Because of the absence of availability of PPS polymer sample with a considerably larger crystallite size to measure b, we assumed that the value of b determined on the basis of a silicon (Si) standard when evaluated under similar WAXS instrument parameters would be sufficient. On the basis of the Si standard, b was found to be equal to 0.6281°.

Long period. The *long period* is the mean repeat distance of the crystal lamellae in the direction of the fiber axis and is given by Eq. (11):

$$L = \frac{2\pi}{\mathbf{q}_{\max}} \tag{11}$$

where $\mathbf{q}_{\max}$ corresponds to the intensity maximum of the scattering vector ($\mathbf{q}$) in the Lorentz-corrected intensity profiles obtained with SAXS. Using the two-phase semicrystalline model, we calculated the lamellar thickness (l) in the direction of fiber axis, termed as the *crystal thickness* herein, from the long period by multiplying the fraction of crystallinity (X_c) with Eq. (12):

$$l = LX_c \tag{12}$$

At the same time of WAXS measurements, X-rays diffracted at smaller angles were detected by a two-dimensional detector for scattering pattern image acquisition. The sample-to-detector distance was 1.5 m. A MathCAD data treatment program developed by Schreiber[23] was used to convert the SAXS patterns into plots of intensity versus scattering vector ($\mathbf{q}$).

RESULTS AND DISCUSSION

Differences in the MW of the PPS resins used were discussed in our earlier publication[9] in terms of the melt flow index (MFI). For the majority of the results discussed next, unless otherwise stated specifically, the as-spun fibers used were manufactured at a take-up speed of 1750 mpm with a throughput of 12 g/min/12 holes and at an extrusion temperature (ET) of 315°C. For the purposes of draw-annealing experiments, AT was kept constant at 150°C.

Factors influencing the draw-annealed fiber structure and properties

Effect of MW

The fibers that are discussed here were drawn at a DT equal to 90°C and annealed further. The leverage plot of the influence of MW ($\propto 1/\text{MFI}$) on the draw-annealed fiber tenacity and breaking elongation is shown in Figure 4. The leverage plots were constructed with statistics software JMP 8.0 (SAS Institute, Inc., Cary, NC). The solid line in the leverage plots is the best fit based on the data points, and the dotted lines indicate 95% confidence limits. It is apparent from the figure that the higher the polymer MW, higher was the tenacity and the lower was the

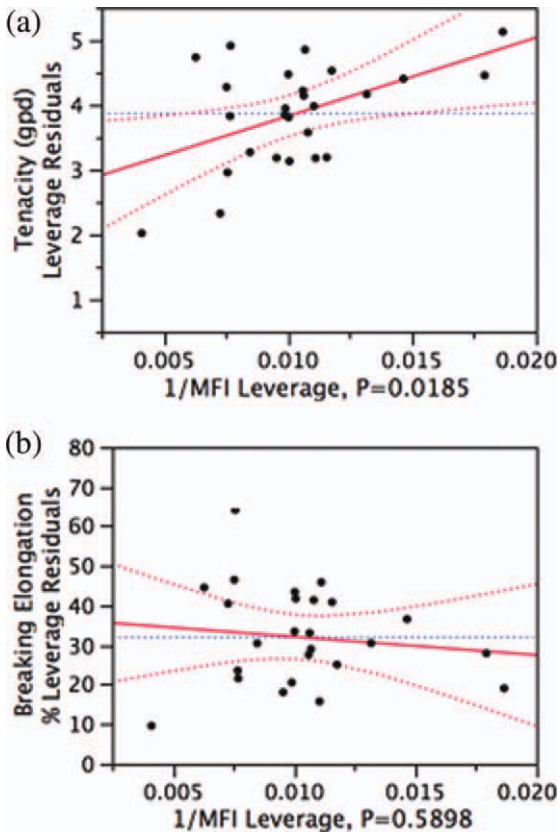

Figure 4 Effect of the polymer MW on the draw-annealed fiber tenacity and elongation. [Color figure can be viewed in the online issue, which is available at wileyonlinelibrary.com.]

breaking elongation of the DA fiber. No significant change was observed in the tensile modulus as a function of polymer MW (Fig. 5) when it was drawn at a DT of 90°C. The tenacities and tensile moduli of these draw-annealed fibers were substantially higher than those of the corresponding as-spun fibers reported in our earlier publication.[9] The WAXS pinhole patterns of these fibers are shown in Figure 6. Δn and the degree of crystallinity are plotted in Figure 7(a), and the f_c and f_{am} values are plotted in Figure 7(b). Although the crystallinity data plotted in Figure 7(a) were obtained from DSC experiments, the level of crystallinity calculated from WAXS for

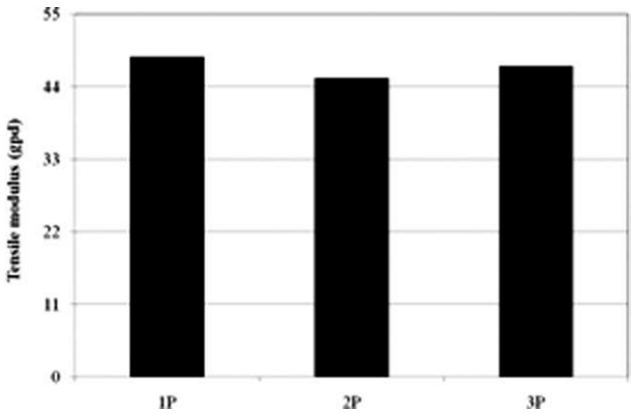

Figure 5 Tensile modulus of the draw-annealed fibers from various MW polymers (DT = 90°C).

these and other samples, which will be discussed further, was in close agreement with that of DSC. The degree of crystallinity [Fig. 7(a)] did not show a considerable change (30–34%); however, Δn [Fig. 7(a)] and f_{am} [Fig. 7(b)] increased with increasing MW. Therefore, the observed increase in tenacity and decrease in breaking elongation with increase in MW could be attributed to improvements in the molecular orientation, more so in the amorphous region at a similar level of crystallinity. An increase in the strength of fibers with an increase in MW in the case of other polymers was reported by Termonia and Smith.[24] The WAXS patterns in Figure 6 and the decreasing trend in f_c [Fig. 7(b)] with an increase in polymer MW indicated that 90°C was not the optimum DT for all of the as-spun fibers, and a higher DT was needed as the polymer MW, from the which the fibers were spun, increased. This could be explained on the fact that and the polymer MW, higher it possesses more chain entanglements the sufficient chain mobility required for stretching happens at higher temperatures.

Effect of the melt-spinning take-up speed

Figure 8 shows the draw-annealed fiber tenacities of the as-spun fibers spun at different take-up speeds and drawn at a 100°C temperature from polymers 1P

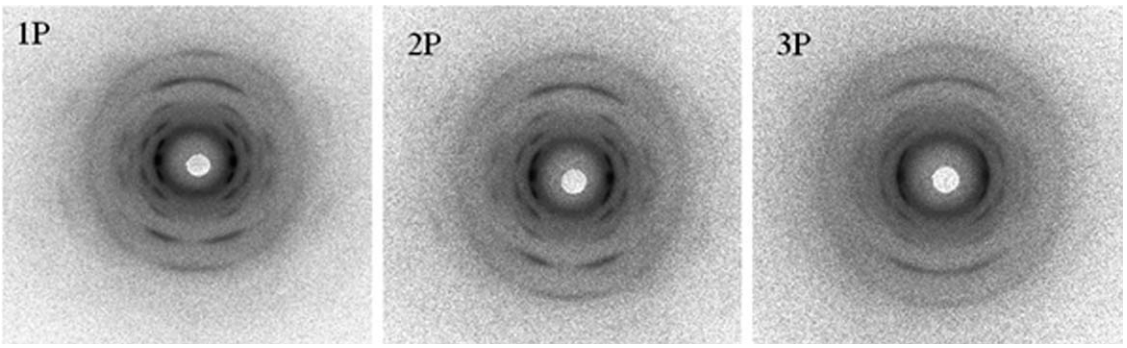

Figure 6 Effect of the polymer MW on the structural development in the drawn fibers (DT = 90°C, vertical fiber axis).

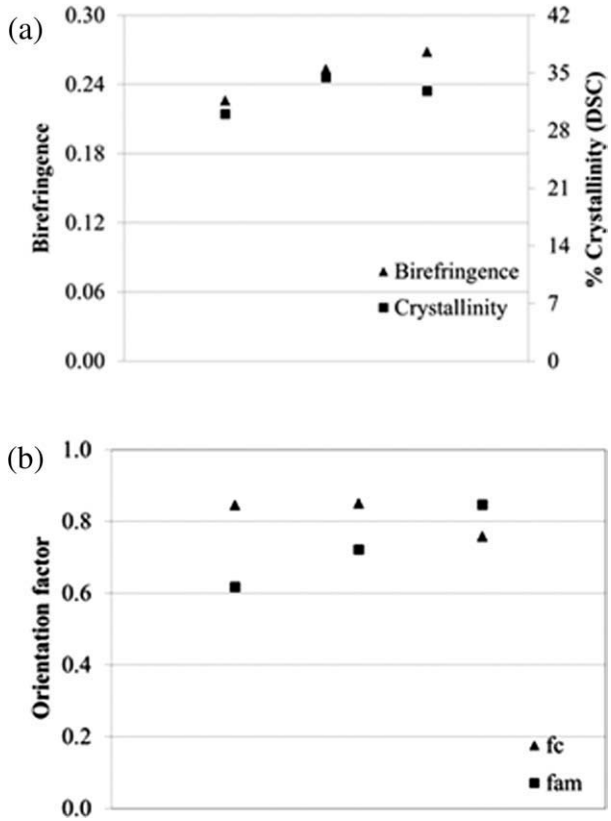

Figure 7 Influence of the polymer MW on the draw-annealed fiber morphology (DT = 90°C).

and 3P. The throughput was 12 g/min/12 holes, and ET during melt spinning is provided in the figure caption. In the case of polymer 1P [Fig. 8(a)], the draw-annealed fiber tenacity was maximum from the fiber spun at a higher take-up speed. For polymer 3P, upon extrusion at 315 and 340°C, the take-up speeds exhibited little influence, with a maximum fiber tenacity around 1750 mpm [Fig. 8(b,c)]. This indicated that the optimum spinning conditions for achieving higher tenacities in the drawn yarn may be different for polymers with different MWs. This behavior may be a combined effect of the level of molecular orientation and the crystallinity in the as-spun fiber and the number of chain entanglements.

Effect of DT

Fiber morphology and properties. Figure 9 shows the effect of DT on the tensile properties of DA fibers spun from three polymer types. All of these fibers were melt-spun at a medium take-up speed of 1750 mpm. The throughput and ET were 12 g/min/12 holes and 315°C, respectively. For a given polymer, as the DT increased above the glass-transition temperature, the tenacity first increased and then started decreasing with a considerable drop in tenacity at elevated DTs [Fig. 9(a)]. Up to optimum DTs, the tenacities of the DA fibers were substantially higher than those of the parent as-spun fibers. However, at extremely elevated temperatures, the tenacities fell down at par or even below that of the corresponding as-spun fibers. The DT at which the maximum in tenacity occurred shifted toward higher temperature with increasing MW. This observation supported our earlier statement that the optimum DT may be higher for fibers spun from high-MW polymers. Polymer 3P exhibited better tenacities over a wider DT range than the lower MW polymers, 1P and 2P. Figure 9(b) shows that the fiber breaking elongation decreased considerably upon drawing compared to the as-spun fiber and did not change much over the range of DTs. This indicated that, beyond the optimum DT, the fibers became increasingly weak. Above the DTs plotted in Figure 9, the fibers became so weak that they could not be pulled off from the first draw roll; this made drawing very difficult. Carr and Ward[3] reported an inability to draw PPS

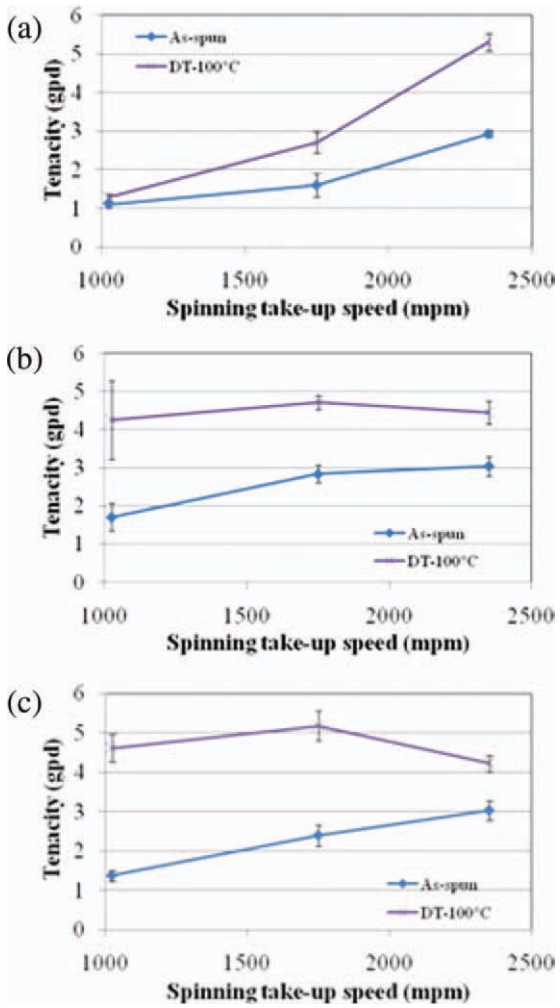

Figure 8 Effect of the fiber spinning take-up speed on the drawn fiber properties (a) 1P ET = 315°C, (b) 3P ET = 315°C, and (c) 3P ET = 340°C. [Color figure can be viewed in the online issue, which is available at wileyonlinelibrary.com.]

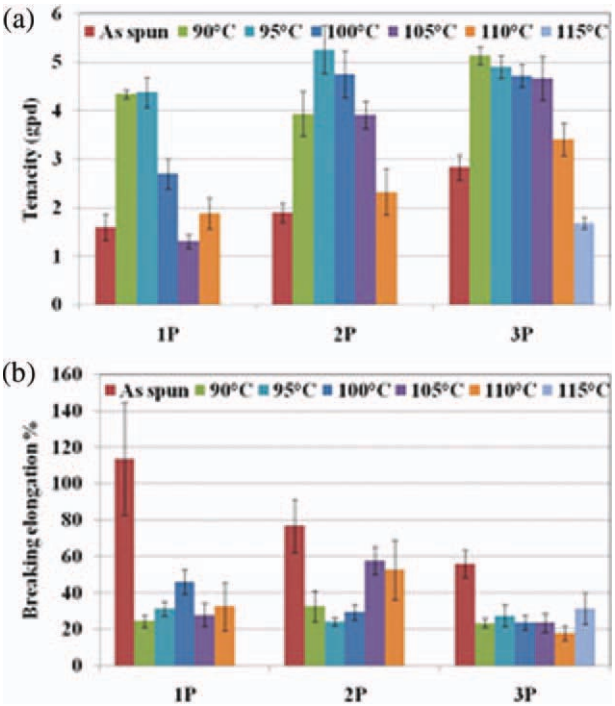

Figure 9 Effect of DT on the fiber properties: (a) tenacity and (b) elongation. [Color figure can be viewed in the online issue, which is available at wileyonlinelibrary.com.]

fibers beyond the DT of 100°C because of filaments sticking to the draw rolls. The probable reason for such difficulty in drawing at higher DTs is discussed subsequently. Figure 10 makes it clear that, with the increase in DT, the tensile modulus decreased in all of the cases, unlike tenacity, which went through a maximum. These changes in the tensile properties could be explained by the draw-annealed fiber morphologies, whereas the drawing behavior could be explained by the as-spun fiber morphologies and is discussed in the following text.

For a given polymer, compared to the as-spun fibers, the DA fibers possessed a better crystalline orientation (Fig. 11), higher Δn [Fig. 12(a)], and higher crystallinity [Fig. 12(b)]. With an increase in DT, Δn of the DA fibers went through a maximum [Fig. 12(a)] for each of the polymers. Comparatively, the crystallinity levels did not show considerable changes [Fig. 12(b)], although they decreased slightly at elevated DTs. In comparison with the as-spun fibers, the diffraction patterns shown in Figure 11 and the diffractograms shown in Figure 13 indicate that the reflections from planes (110) and (200) were better separated in the DA fibers than in as-spun fibers; this suggested a higher degree of crystalline orientation in the DA fibers. The enhanced molecular orientation along the fiber axis in the DA fibers compared to that in the as-spun fibers resulted in considerable improvements in the tenacity [Fig. 9(a)] and tensile modulus (Fig. 10) and decreases in the breaking elongation [Fig. 9(b)] of DA fibers up to an optimum DT.

Up to the optimum DT, f_c [Fig. 14(a)] increased, and f_{am} [Fig. 14(b)] was also substantially higher, around 0.8. The long period and crystal thickness plots, as shown in Figures 15 and 16, respectively, indicated that these parameters went through a minimum with increasing DT. The minimums in the long period and crystal thickness suggested smaller crystals. At a fairly similar degree of crystallinity, smaller crystals suggest an increase in the number of crystals and number of intercrystalline regions. Peterlin[25] described such phenomenon in terms of an increasing fraction of microfibrils. Therefore, taut tie chains, with a greater number of them between crystallites and oriented highly ($f_{am} \approx 0.8$) along the fiber axis, result in an increase in the fiber tenacity and a decrease in the breaking elongation up to an optimum DT.

A substantial decrease in the fiber tenacity at elevated DT could also be explained on the basis of the fiber structure. At elevated DT, a considerable loss of molecular orientation was observed, both in the crystalline and amorphous regions (Fig. 14), with a substantial decrease, particularly in the amorphous regions. The probable cause for a loss of molecular orientation may have been slippage of the chains past each other and coiling thereafter, as could be deduced from the increasingly viscous flowlike behavior of the chains with increasing temperature.[9] Above a certain temperature, the long period (Fig. 15) and crystal thickness (Fig. 16) increased and, thereby, indicated the development of larger crystals beyond those DTs. At comparable or somewhat lower levels of crystallinity, this suggested larger intercrystalline spaces and, thus, a lower number of taut tie chains. Therefore, a poorly oriented [$f_{am} \approx 0.4$ in Fig. 14(b)] and lower number of tie chains led to a decrease in the tenacity when drawing was above the optimum DT.

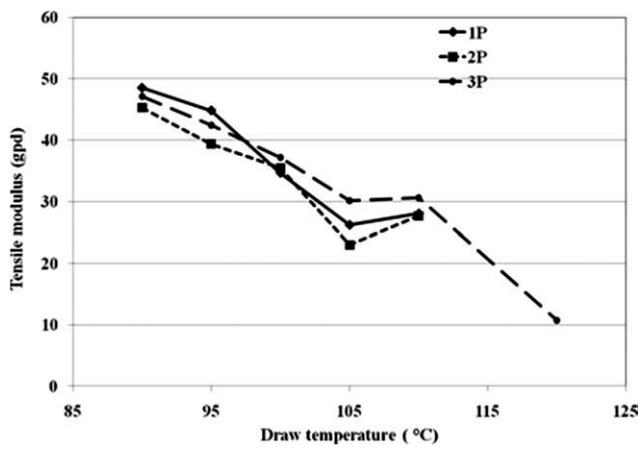

Figure 10 Effect of DT on the tensile modulus.

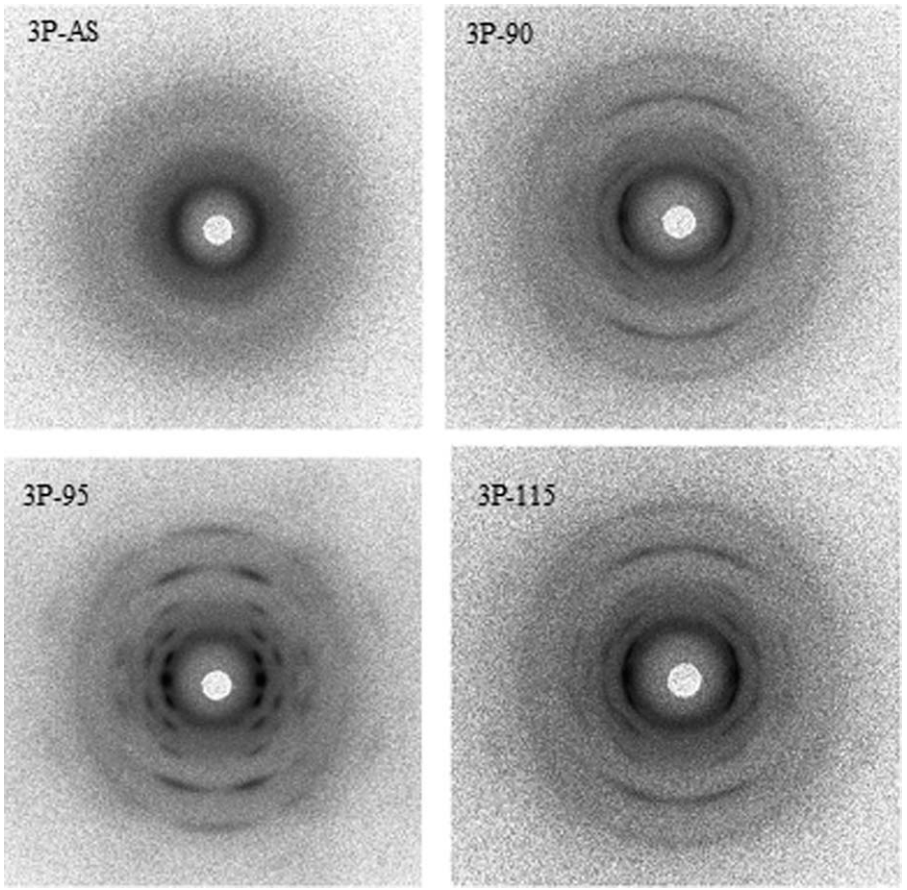

Figure 11 WAXS pinhole patterns of the drawn fibers as a function of DT.

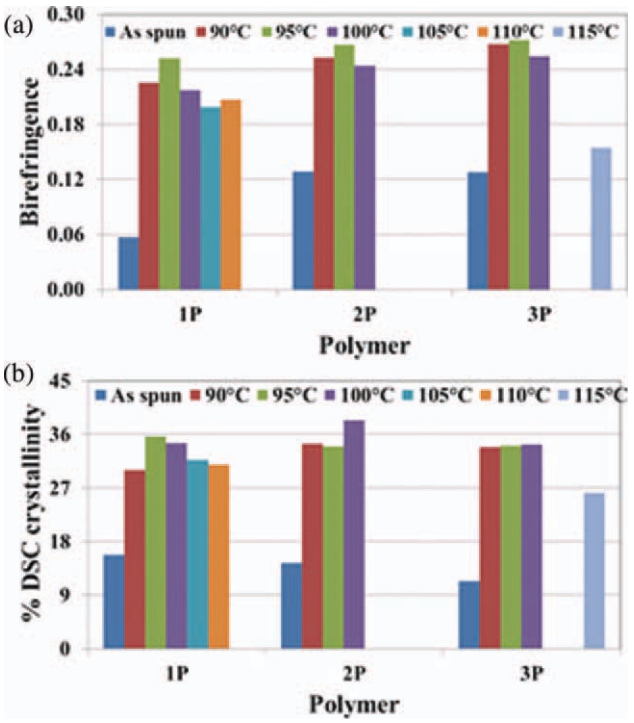

Figure 12 Effect of DT on the fiber morphological properties: (a) Δn and (b) crystallinity. [Color figure can be viewed in the online issue, which is available at wileyonlinelibrary.com.]

Unlike the fiber tenacity, which went through a maximum, the tensile modulus of the DA fibers decreased continuously with increasing DT. A considerable drop in the modulus at DTs beyond the optimum DT could be ascribed to poorly oriented tie chains under these process conditions. Figure 17 shows the relationship between the tensile modulus

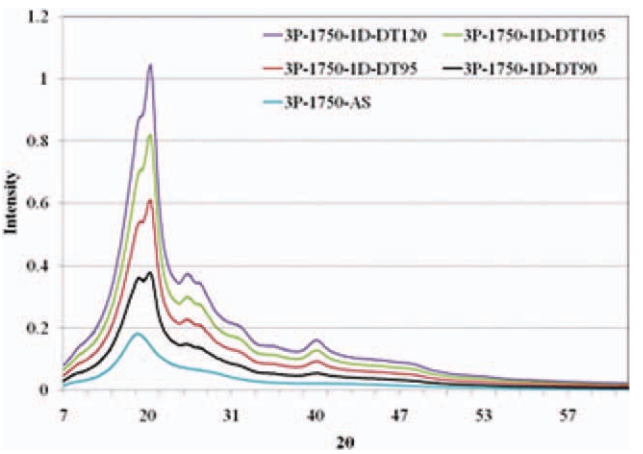

Figure 13 WAXS diffractograms of the as-spun and draw-annealed fibers (polymer 3P). [Color figure can be viewed in the online issue, which is available at wileyonlinelibrary.com.]

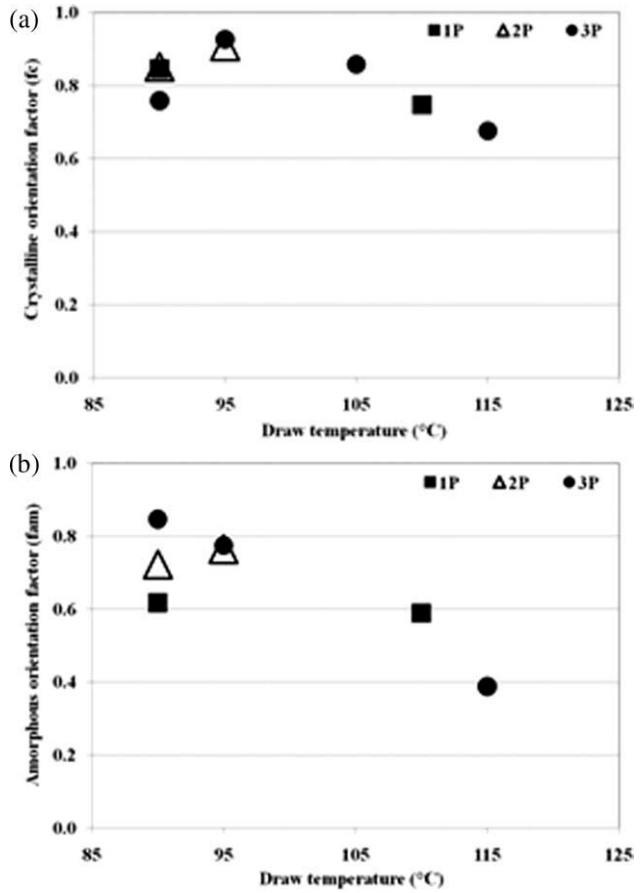

Figure 14 Effect of DT on the molecular orientation: (a) f_c and (b) f_{am}.

and several morphological properties of the fibers. The solid lines are fitted trend lines, and the regression coefficient (R^2) for each of the trend lines is also shown. The best relation was observed between the modulus and f_{am}. A similar strong relationship between f_{am} and the tensile modulus was reported by Yamada et al.[26] in the case of highly oriented polypropylene films. Figure 14(b) shows that f_{am}

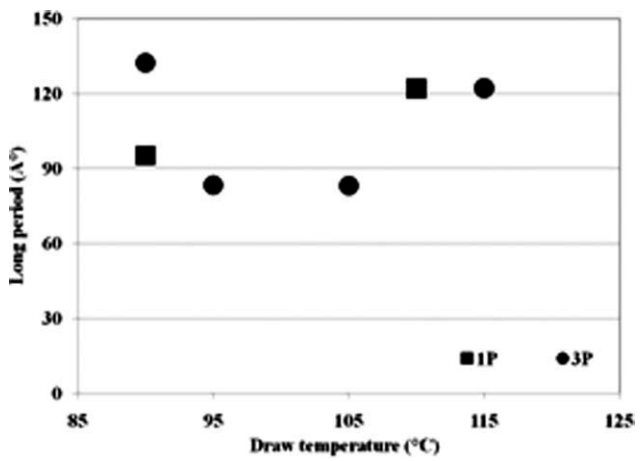

Figure 15 Effect of DT on the long period (polymer 3P).

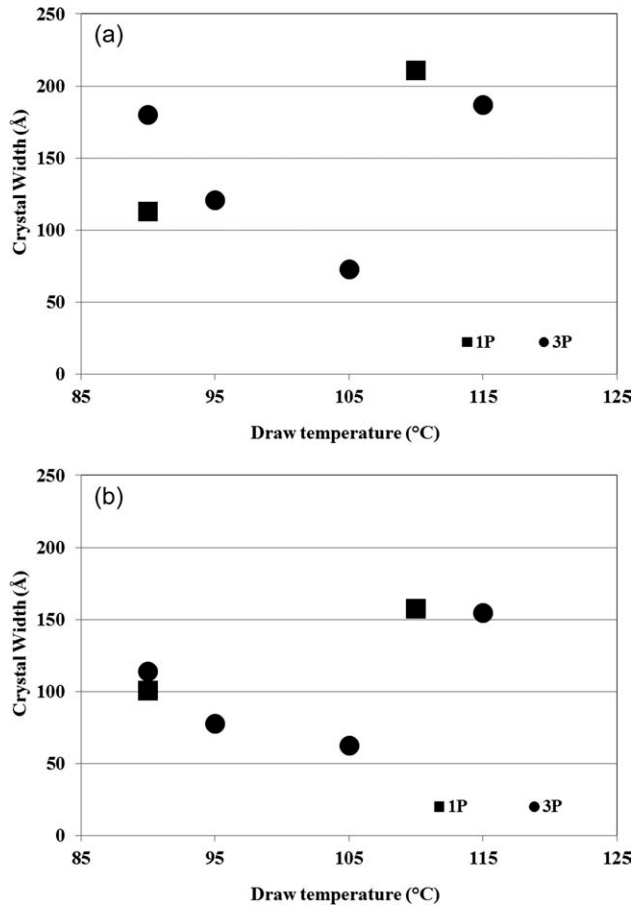

Figure 16 Effect of DT on the crystal width (perpendicular to fiber axis): (a) plane (110) and (b) plane (200).

decreased with increasing DT, even in the region up to optimum DT. Considering the strong and direct correlation between the tensile modulus and f_{am}, it can be stated that with increasing DT, the decrease

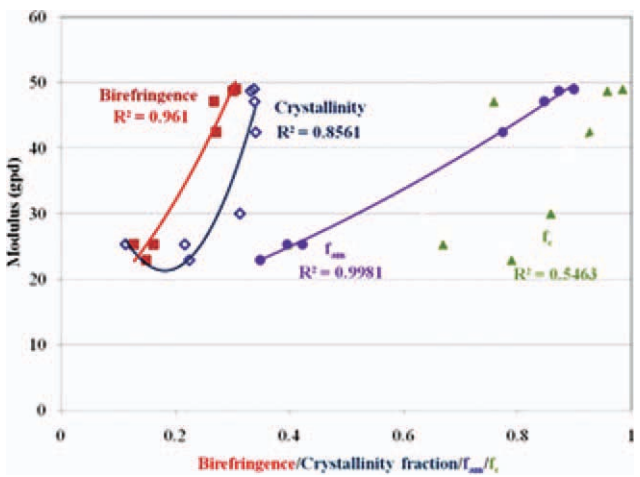

Figure 17 Effect of the morphological properties on the fiber tensile modulus (the data correspond to fibers spun from all four polymers draw-annealed under different conditions). [Color figure can be viewed in the online issue, which is available at wileyonlinelibrary.com.]

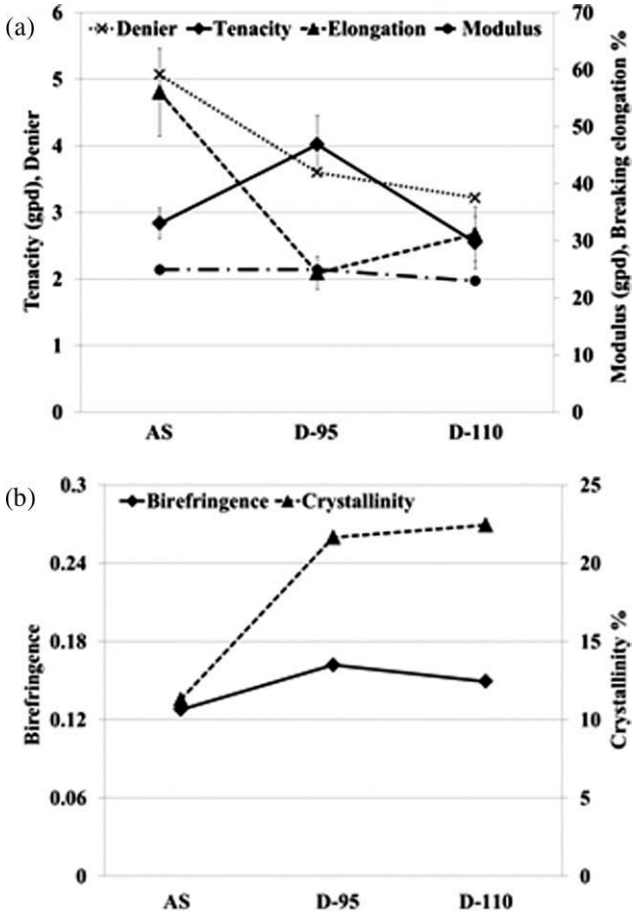

Figure 18 Effect of DT on the fiber structure and properties.

in f_{am} [Fig. 14(b)] caused the tensile modulus to decrease (Fig. 10).

To separate the effects of annealing from the effects of drawing, we carried out experiments by drawing the fibers at 95 and 110°C and not annealing them further. The fiber structure–property results are given in Figure 18. The solid lines are shown for better clarity of trend visualization. It becomes clear from Figure 18(a) that the fiber denier decreased when drawn at 110°C as compared to 95°C and indicates that drawability was higher at higher DTs, as expected because of the greater chain mobility at higher temperatures. However, the tenacity showed a considerable decrease when the fibers were drawn at 110°C than when they were drawn at 95°C.

A decrease in Δn was observed at higher DTs [Fig. 18(b)]. The orientation factors, f_c and f_{am}, in fibers drawn at 95°C were found to be 0.67 and 0.42, respectively. The corresponding values in the fibers drawn at 110°C were 0.79 and 0.35. The tensile modulus of drawn fibers was similar to that of the as-spun fibers [Fig. 18(a)] for the reasons that f_{am} was similar between the as-spun (0.39) and drawn fibers. A considerable decrease in the tenacity could be explained by a decrease in the amorphous orientation in the fiber when it was drawn at a higher DT. These experiments suggest that even after the annealing effects were excluded, changes in the fiber structure and properties followed similar trends, as discussed earlier. Hence, the discussion pertaining to changes in the fiber structure and properties as a function of DT in the case of the draw-annealed fibers seems to be valid. The influence of annealing on the development of molecular orientation, especially in the amorphous region, will be discussed in a subsequent publication, in which we will report on the role of two-zone drawing and annealing in the structure–property development in PPS fibers.

Drawing process performance. The range of DTs to obtain a fair level of fiber tenacities was wider for fibers spun from high-MW polymers. It was reported in our earlier publication[9] that viscous flowlike behavior in as-spun fibers produced under similar processing conditions occurred at higher temperatures in fibers spun from high-MW polymers. The limiting case of such viscous flow will be the sticking of the fibers to the draw roll, an observation made in this investigation and that by Carr and Ward[3] above a certain DT. During the thermomechanical analysis of as-spun fibers,[9] the viscous flow of fibers was attributed to the absence or lower number of physical crosslinks. The probability of increasing the presence of physical crosslinks would be higher in fibers spun from high-MW polymers spun under similar conditions. Therefore, a wider range of DTs for the satisfactory processing of as-spun fibers manufactured from high-MW resins could be well correlated to a higher number of physical crosslinks in these fibers.

CONCLUSIONS

The optimum drawing performance was achieved at a DT around 95°C. Considerable improvement in the fiber tenacities was reported upon DA under suitable drawing conditions as compared to their as-spun counterparts, and the fiber tenacities achieved were around 5 g/den. DTs beyond the optimum deteriorated the fiber tensile properties. The increase in tenacity and decrease in breaking elongation up to an optimum DT was correlated to an increasing number of taut tie chains oriented along the fiber axis. A decrease in the tenacity beyond an optimum DT was correlated to a lesser number of and poorly oriented tie chains. The decrease in the tensile modulus was attributed to a decrease in the orientation of noncrystalline regions. Depending on the polymer MW, different paths were shown to exist in the achievement of higher tenacities in the draw-annealed fibers by a combination of optimum spinning and drawing

process parameters. A wider drawing process window for high-MW polymers and for high-speed spun fibers was shown to be related to the physical crosslinks in the fibers.

The authors sincerely thank Ticona Polymers, a business of Celanese Chemicals, for funding this research project and for supplying proprietary Fortron® PPS resins for the study. Continued interaction with Manoj Ajbani, Ke Feng, and Lisa Baker (all from Ticona Polymers) is gratefully acknowledged. The funding support for one of us (P.G.) by the Center for Materials Processing at The University of Tennessee, Knoxville, during the initial years of graduate studies is also highly appreciated.

References

1. Jog, J. P.; Nadkarni, V. M. J Appl Polym Sci 1985, 30, 997.
2. Song, S. S.; White, J. L.; Cakmak, M. Int Polym Process 1989, 2, 96.
3. Carr, P. L.; Ward, I. M. Polymer 1987, 28, 2070.
4. Padibjo, S. R.; Ward, I. M. Polymer 1983, 24, 1103.
5. Krins, B.; Feijen, H. H. W.; Heuzeveldt, P.; Vieth, C.; Diolen, R. E. (To Industrial Fibers Bv Netherlands.) Can. Pat. 2,601,751 (2006).
6. Bratukhin, A. V.; Isaeva, V. I.; Filbert, D. V.; Semenova, T. P. In Khimicheskie Volokna; All-Union Scientific Research Institute for Synthetic Fibres: 1974; p 53.
7. Murthy, N. S.; Elsenbaumer, R. L.; Frommer, J. E.; Baughman, R. H. Synth Met 1984, 9, 91.
8. Suzuki, A.; Kohno, T.; Kunugi, T. J Polym Sci Part B: Polym Phys 1998, 36, 1731.
9. Gulgunje, P. V.; Bhat, G. S.; Spruiell, J. E. J Appl Polym Sci, 2011, 122, 3110.
10. Morton, R. W.; Simon, D. E.; Geibel, J. E.; Gislason, J. J.; Heald, R. L. In Advances in X-Ray Analysis; International Centre for Diffraction Data: Newtown Square, PA, 2001; Vol. 44, p 103.
11. Tabor, B. J.; Magre, E. P.; Boon, J. Eur Polym J 1971, 7, 1129.
12. Alexander, L. E. In X-ray Diffraction Methods in Polymer Science, 3rd ed.; Krieger, R. E., Ed.; Krieger: Malabar, FL, 1979; p 248.
13. Spruiell, J. E.; Janke, C. J. A Review of the Measurement and Development of Crystallinity and Its Relation to Properties in Neat Poly(Phenylene Sulfide) and Its Fiber Reinforced Composites; ORNL/TM-2004/304; Oak Ridge National Laboratory: Oak Ridge, TN, 2004.
14. Stein, R. S. J Polym Sci 1958, 31, 327.
15. Hermans, P. H.; Hermans, J. J.; Vermaas, P.; Weidinger, A. J Polym Sci 1948, 3, 1.
16. Stein, R. S.; Norris, F. H. J Polym Sci 1956, 6, 231.
17. Maemura, E.; Cakmak, M.; White, J. L. Int Polym Process 1988, 2, 79.
18. Carr, P. L.; Ward, I. M. Polymer 1987, 28, 2070.
19. Stein, R. S. In U.S.–Japan Seminar on Polymer Physics (Journal of Polymer Science C15); Stein, R. S., Onogi, S. Eds.; Interscience: New York, 1966; p 185.
20. Scherrer, P. Gottinger Nachrichten 1918, 2, 98.
21. Klug, H. P.; Alexander, L. E. X-Ray Diffraction Procedures; Wiley: New York, 1954; Chapter 9.
22. Schoening, F. R. L. Acta Cryst 1965, 18, 975.
23. Schreiber, S. L. Thesis, University of Tennessee, Knoxville, 1998.
24. Termonia, Y.; Smith, P. Polymer 1986, 21, 1845.
25. Peterlin, A. Text Res J 1972, 42, 20.
26. Yamada, K.; Kamezawa, M.; Takayanagi, M. J Appl Polym Sci 1981, 26, 49.